Data Acquisition System for Monitoring JNEC Distribution Network

Dawa Choden[1*], Deki Dema[2], Sonam Yuden[3], Thinley Tobgay[4]

[*1, 2, 3,4] Department of Electrical and Electronics Engineering, Jigme Namgyel Engineering College, Royal University of Bhutan

E-mail: 05220023.jnec@rub.edu.bt[1*], 05220002.jnec@rub.edu.bt[2], 05210354.jnec@rub.edu.bt[3], thinleytobgay.jnec@rub.edu.bt[4]

Received: 24 May 2026; Revised: 06 July 2026; Accepted: 08 August 2026; Published: 13 August 2026

Abstract

Reliable electrical parameter monitoring is essential for managing institutional distribution networks; however, conventional power quality analysers remain cost-prohibitive for campus-wide deployment. The design and implementation of a low-cost, IoT-based Data Acquisition System (DAQ) for real-time monitoring of the JNEC campus distribution network is presented and its experimental validation is carried out. The system consists of a voltage sensor (ZMPT101B), a current sensor (ACS712), signal acquisition module (Arduino UNO), wireless module (ESP32), and cloud platform modules (Firebase, ThingSpeak). Validation was performed by comparing the multi-parameter acquisition modes of the Multimeter with a Fluke 435 Series II Power Quality Analyser and a reference meter (MECO PM-VAC-5R) with resistive, capacitive and inductive loads. Under steady-state conditions, the system successfully reached the IEC Class 0.5 performance level in terms of Mean Absolute Error (MAE), with an error of less than 1.73% and Root Mean Square Error (RMSE), less than 2.06%, relative to the reference instruments for voltage and apparent power measurements under inductive loading. The voltage Total Harmonic Distortion (THD-V) and current Total Harmonic Distortion (THD-i) levels of the inductive load were calculated using MATLAB-based Fast Fourier Transform (FFT) analysis: The THD-V level was 15.38%, which was measured in the transient mode of the motor startup condition, and the THD-i level was 84.16%, which was also measured in transient mode of the motor startup condition, and both were within IEEE Std 519-2014 characterisation criteria. The proposed system shows that a scalable and inexpensive IoT DAQ platform can provide an applied engineering education with professionally relevant power quality data for electrical infrastructure management of a campus.

Keywords: *Internet of Things (IoT), Electrical Parameter Monitoring System, Arduino Uno, ESP32 Wi-Fi Module, ZMPT101B Voltage Sensor, ACS712 Current Sensor, Firebase, ThingSpeak*

1. INTRODUCTION

Institutional electrical distribution networks, especially those that supply educational campuses, must undergo constantly changing loads such as computer labs, air-conditioning systems, workshop equipment, and lighting systems. These loads, combined, contribute to power quality problems such as voltage fluctuations, harmonic distortion, power factor issues and reactive power imbalance which affect the system efficiency, causes degradation of the equipment and contribute to operational losses of energy in the system (Hamzah & Hassan, 2024). In the case of Jigme Namgyel Engineering College (JNEC), there is no dedicated real-time monitoring system; this results in such disturbances spreading undetected and poses an operational risk to critical laboratory equipment, as well as driving up maintenance costs.

Conventional power quality analysers, including the Fluke 435 Series II, which is compliant with IEC 61000-4-30 and IEEE Std 1159-2019 and can measure voltage, current, harmonics, frequency and power factor, are able to measure high-accuracy reference measurements but are not cost-effective for deployment at the distributed campus level (Sahabudin et al., 2024). The economic constraint has driven the growing interest in cost-effective monitoring solutions for IoT networks which are based on low-cost sensors and cloud services to provide similar power quality monitoring functions at a reduced cost (Ferdiansyah & Wardana, 2025; Krishna Challa et al., 2020).

The use of embedded microcontrollers (Arduino Uno ATmega328P and ESP32 Wi-Fi) and voltage sensors (ZMPT101B) along with current sensors (ACS712 Hall-effect) has made the acquisition of power parameters on the basis of the IoT platform a viable solution (Ayob et al., 2025; Pardede & Brahmana, 2023). However, most of the existing implementations are only able to measure basic voltage and current values, and do not measure other important parameters such as harmonics, frequency variation, reactive power, and power factor. (Hamzah & Hassan, 2024) Additionally, there is little mention of campus scale multi-point deployment with wireless cloud transmission in the literature.

In the light of such identified gaps in the context of JNEC, this paper proposes a multi-parameter IoT based DAQ system, which acquires seven electrical parameters simultaneously, transmits the data wirelessly to cloud platforms in real time, and does FFT based harmonic analysis according with IEEE Std 519-2014. Specific contributions of the present work include: (1) an IoT sensing architecture that combines Arduino Uno and ESP32 with ZMPT101B and ACS712 sensors for multi-parameter sensing; (2) experimental validation of multi-parameter sensing using the proposed sensing architecture in comparison with the reference instruments, demonstrating MAE below 1.73% for three categories of load; and (3) the power quality profile characterisation of inductive motor load using a MATLAB harmonic analysis model for the experimental validation of the proposed architecture.

2. LITERATURE REVIEW

2.1. Motivation for IoT-Based Monitoring

In the educational environment, a growing number of non-linear loads and sensitive loads has placed a pressing demand for real-time monitoring of electrical parameters at all times. These loads cause disturbances to the system, which can lead to decreased system efficiency and increased equipment wear (Hamzah & Hassan, 2024). Ferdiansyah and Wardana (2025) showed the feasibility and affordability of applying IoT-based systems for energy management in resource constrained institutional settings, while Krishna Challa et al. (2020) validated the ability of wireless distributed sensing architectures for acquiring and transmitting electrical parameters to the centralised monitoring platforms. In sum, these studies have demonstrated that an IoT-based DAQ system is a viable approach to better the electrical system awareness in the campus like JNEC where the commercial analysers are cost prohibitive.

2.2. Architectures for Sensing and Hardware

The ZMPT101B voltage sensor and ACS712 Hall sensor current sensor are two popular sensors for low cost embedded monitoring systems at the sensor level. Ayob et al. (2025) designed a three-phase power measurement system with ESP32, ZMPT101B sensors, and ACS712 sensors, which minimizes the errors in the measurement system under 2% using cross-correlation-based power factor calculation. The ACS712 sensor will give an analog output voltage proportional to the current, which is then converted to a digital value by the microcontroller's ADC. The accuracy of this sensor is very sensitive to calibration and external interference (Sahabudin et al., 2024). The error value if not calibrated is as high as 28% and when using the appropriate calibration constant the maximum error value is reduced to 3.43% (Pardede & Brahmana, 2023). In addition, Wibowo et al. (2024) found that the current measurement standard deviation of external 16-bit ADC is 86.8 mA, which is lower than the standard deviation of the measurement carried out by Arduino's built-in 10-bit ADC of 486 mA, making external 16-bit ADC useful in obtaining accurate current measurements.

2.3. Research Gaps

Although efforts have been made to monitor through IoT various aspects of the global environment have remained crucial themes that need to be addressed in the existing literature to motivate the development of the JNEC DAQ system. Although significant progress has been made in the monitoring of various aspects of the global environment through IoT, there are three critical gaps in the existing literature that motivate the development of the JNEC DAQ system. Most of the systems measure only voltage and current, and not include harmonics, frequency variation, reactive power and power factor which are crucial for an extensive evaluation of power quality on a campus (Hamzah & Hassan, 2024; Ayob et al., 2025). Second, current solutions mostly focus on monitoring for a single appliance or single phase in a residential setting, whereas for monitoring in institutional distribution systems, scalability is required, as there are numerous appliances or phases to be monitored, and wireless connectivity is essential (Ferdiansyah & Wardana, 2025). Third, the ACS712 sensor was only rarely applied without the signal conditioning and calibration corrections that Pardede and Brahmana (2023) and Wibowo et al. (2024) have suggested, which restricts the reliability of the application in professional use. The proposed JNEC DAQ system fills all three gaps and integrates the multi-parameter acquisition, calibrated sensor conditioning and wireless transmission to the cloud in a single scalable system.

3. METHODOLOGY

The system development followed a structured sequential methodology encompassing literature review, circuit design, simulation-based verification, sensor calibration, hardware prototyping, and experimental validation. Fig. 1 illustrates the overall development workflow.

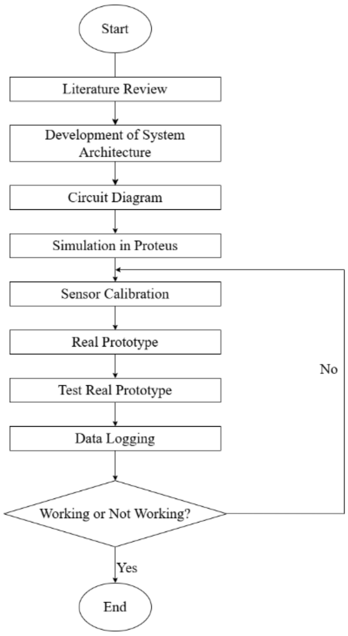

***Fig. 1**: System Development Methodology*

3.1. System Architecture

The hardware architecture follows a three-tier sensing model that ensures structured and efficient signal flow from the physical electrical network to the cloud, as illustrated in Fig. 2.

Sensing Layer: The ZMPT101B voltage sensor and ACS712 current sensor interface directly with the monitored circuit, converting electrical signals into analogue voltage outputs compatible with the Arduino ADC input range (0 – 5 V).

Processing Layer: The ATmega328P-based Arduino Uno microcontroller samples the sensor outputs at a rate satisfying the Nyquist criterion, computes RMS values, active power, reactive power, apparent power, power factor, and supply frequency using the discrete algorithms detailed in Section 3.4, and applies calibration constants to correct sensor offsets.

Communication Layer: The ESP32 Wi-Fi module receives processed data from the Arduino via serial communication and transmits it wirelessly over the 2.4 GHz IEEE 802.11 network to Firebase Realtime Database and ThingSpeak cloud platforms for visualisation and archiving.

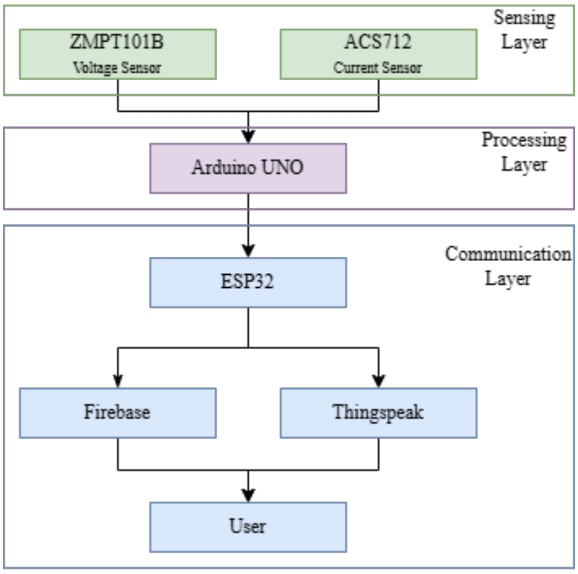

***Fig. 2:** System Architecture*

3.2. Circuit Design and Simulation

The electronic schematic, designed in Fritzing, defines all sensor-to-microcontroller interconnections, including the voltage divider network for the ZMPT101B and the analogue signal path for the ACS712, as shown in Fig. 3. A critical design requirement was ensuring that both positive and negative AC half-cycles were measurable within the Arduino ADC's 0 – 5 V input range; this was achieved by stepping down the voltage signal and applying a 2.5 V DC midpoint bias to shift the AC waveform into the positive ADC window.

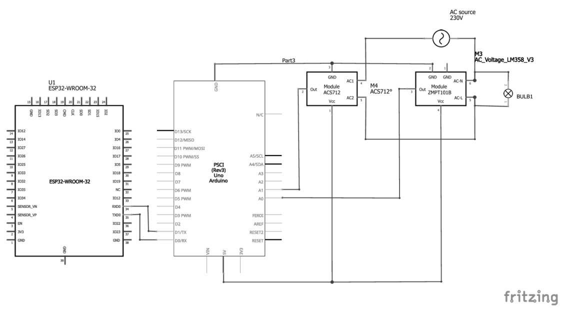

***Fig. 3:** Circuit Diagram*

Prior to hardware fabrication, the circuit was simulated in Proteus software to verify performance of signal conditioning-including amplification gain and low-pass filter cut-off frequency-under representative AC load conditions, as shown in Fig. 4. The simulated waveform was further verified against the physical signal on a digital oscilloscope (Fig. 5), confirming correct AC waveform reconstruction within the ADC acquisition window.

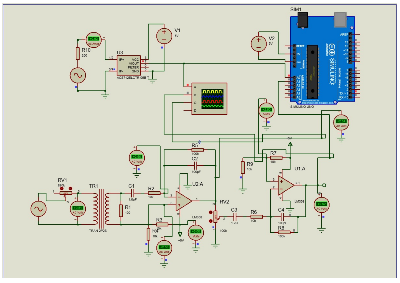

***Fig. 4:** Simulation in Proteus*

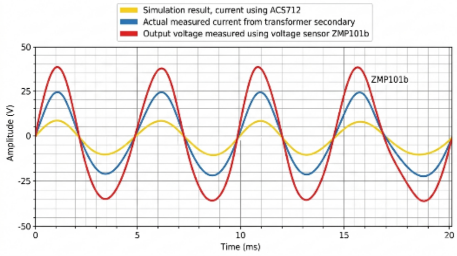

***Fig. 5:** Result from the Digital Oscilloscope*

3.3. Real Prototype

Table 1 lists the hardware components and specifications used in the physical prototype. The assembled prototype integrates all sensing, processing, and communication components on a breadboard, enabling flexible reconfiguration across the three experimental load scenarios, as shown in Fig. 6.

***Table 1:** Materials Required and its specifications*

Sl. No	Name of the material	Specification	Quantity
1	Voltage Sensor	ZMPT101B AC, 5V(DC), 0-250 (AC)	1 No
2	Current Sensor	ACS712 $\pm 5A, \pm 20A$ or $\pm 30A$	1No
3	Arduino UNO	Atmega328P,5V,16 MHz,I2C	1No
4	ESP32	3.3V, 34GPIO pins, 240MHz	1No
5	MECO	MECO PM-VAC-5R	1No
6	Power Quality Analyzer	Fluke 435 Series II PQA	1No
7	Multimeter	CAT III 1000V, CA T IV 600V	1No
8	Breadboard	36 V, ~1A, 2.54 mm, 20–29 AWG	1No
9	Jumper wire	Male-Male / Male-Female / Female-Female, 2.54 mm 22AWG, 10 cm – 30 cm	APR
10	Frequency meter	Digital Frequency Meter, 1 Hz – 50 MHz, 3.3 V – 12 V DC	1No

The physical prototype setup and the hardware wiring diagram are shown below. Fig. 6 shows the physical prototype setup and hardware wiring diagram.

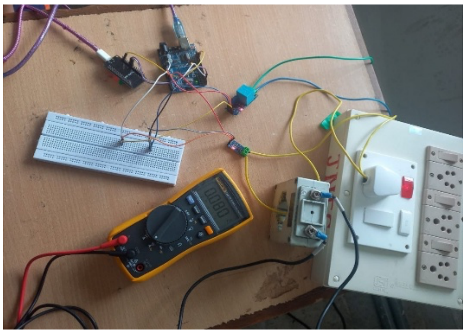

***Fig. 6:** Designed Module*

3.4. Testing of Real Prototype

a. Acquisition of data and computational algorithms

The Arduino firmware samples both sensor outputs at a sampling rate of 9,615 Hz (N = 192 samples per 50 Hz cycle). RMS values are computed from the discrete sample sets using the following equations.

The RMS voltage is calculated as:

$$V_{rms} = \sqrt{\left(\frac{1}{N}\right) \times \sum_{i=1}^{N} V_i^2 \times k_v} \qquad (1)$$

Where:
N= number of samples
V_i = sampled current values
k_v = current calibration factor
This is multiplied by a calibration factor (K).
The RMS current is calculated analogously:

$$\mathrm{I_{rms}} = \sqrt{\left(\frac{1}{\mathrm{N}}\right) \times \sum_{\mathrm{i}=1}^{\mathrm{N}} I_{\mathrm{i}}^2 \times \mathrm{k}_i} \qquad (2)$$

Where:
N= number of samples
I_i = sampled current values
k_i= current calibration factor

Active power P (W) is computed as the average of instantaneous power products;

reactive power Q (VAr), apparent power S (VA), and power factor PF are derived from P, Q, and S using standard single-phase relationships. Supply frequency f (Hz) is extracted via a zero-crossing detection algorithm that timestamps successive positive-to-negative voltage transitions in the firmware interrupt service routine.

3.5. Cloud (Integrate and Visualize)

A three-platform data logging architecture provides real-time monitoring, dashboard visualisation, and long-term archival:

Firebase Realtime Database: Receives parameter updates every second and stores 5-minute summary logs for trend analysis. Fig. 7 confirms successful real-time frequency transmission to Firebase.

ThingSpeak: Provides graphical real-time dashboards for all monitored parameters, enabling visual trend monitoring without dedicated hardware.

Google Sheets: Receives automatically exported monthly summaries for long-term historical reporting and institutional energy auditing.

3.6. Experimental Validation Protocol

Validation was conducted in a controlled laboratory environment using a nominal 230 V, 50 Hz single-phase supply. The DAQ system was compared against two reference instruments operating simultaneously:

Primary Reference: Fluke 435 Series II Power Quality Analyser - high-precision ground-truth measurements for all seven parameters including harmonics.

Secondary Reference: MECO PM-VAC-5R Digital Meter - independent verification of voltage and current readings.

Three load configurations were tested to characterise system performance across diverse power factor and impedance conditions:

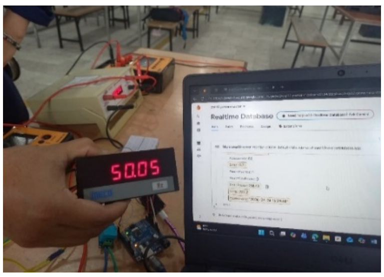

Fig. 7: *Frequency measured by MECO Digital Frequency Meter and Real-time in Firebase*

(i) Resistive load - 1 kVA resistive heating elements (unity power factor, Fig.8)

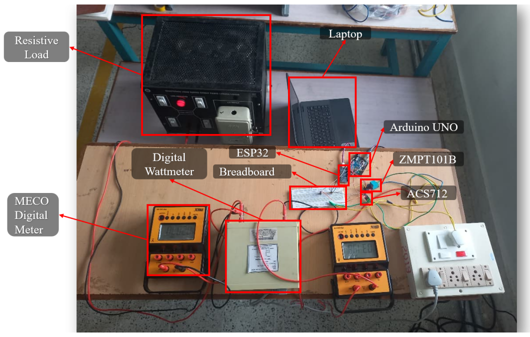

Fig. 8: *Test with resistive load bank*

(ii) Capacitive load - 1 kVA capacitor bank (leading power factor, Fig. 9)

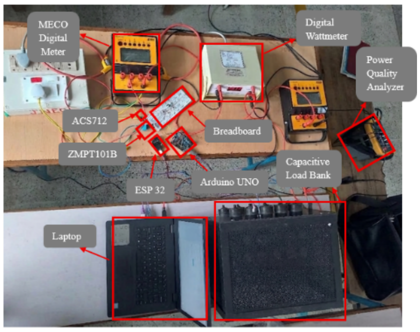

Fig. 9: *Test with capacitive load bank*

(iii) Inductive load - single-phase induction motor via auto-transformer ramp from 0 to 230 V (lagging power factor, Fig. 10)

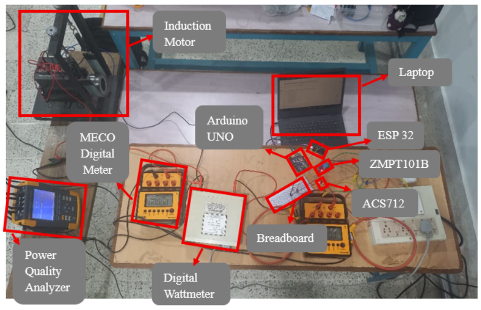

Fig. 10: *Test with single-phase induction motor*

3.7. Performance Metrics

Measurement accuracy was quantified over n = 50 consecutive measurements per parameter using Mean Absolute Error (MAE) and Root Mean Square Error (RMSE):

$$MAE = \frac{1}{n} \times \sum_{i=1}^{n} \left| x_i - x_{ref\,i} \right| \quad (3)$$

$$RMSE = \sqrt{\left(\frac{1}{n} \times \sum_{i=1}^{n} \left| x_i - x_{ref\,i} \right|^2 \right)} \quad (4)$$

Where:
x_i = Measurement given by proposed system (DAQ)
x_{refi} = Measurement given by reference instrument

Percentage MAE and RMSE values are reported relative to the mean reference value to enable cross-parameter comparison.

3.8. Harmonic Analysis Framework

MATLAB-based FFT processing was applied to raw waveform data captured under inductive motor loading. The pre-processing pipeline comprised: (1) motor startup transient removal to isolate steady-state segments; (2) DC offset elimination via mean subtraction; (3) linear detrending to remove residual ramp components; and (4) Hanning window application to reduce spectral leakage. THD was computed up to the 25th harmonic order for both voltage (THD-V) and current (THD-i) and benchmarked against IEEE Std 519-2014 individual harmonic limits.

4. RESULTS AND DISCUSSION

4.1. Measurement Performance by Load Type

Validation was conducted under resistive, capacitive, and inductive load configurations. In every case the DAQ system (device under test) was benchmarked simultaneously against the MECO PM-VAC-5R digital meter and the Fluke 435 Series II Power Quality Analyser (both reference standards) as shown in Table 2.

Table 2: *Instrument Comparison for All Load Types*

Attribute	MECO Clamp Meter	DAQ System	Fluke Power Quality Analyzer
Role	Reference Standard	Device Under Test	Reference Standard
Chart Identifier	Blue (MECO)	Red (DAQ)	Yellow (PQA)
Primary Strength	Voltage & current measurement	Multi-parameter acquisition	Power quality & frequency
Measurement Range	Vrms, Irms and power	All 7 real parameters	All 7 parameters including harmonics

a. Resistive Load Validation

Under resistive loading, the DAQ system tracked the reference instruments closely across all measured parameters. As shown in Fig. 11 and Fig. 12, RMS voltage and RMS current followed the MECO and Fluke PQA traces within their respective tolerance bands throughout the test window (Table 3, Table 4). The comparison against the PQA yielded an overall MAE of 1.73% and an RMSE of 2.06% for voltage, while real power (Fig. 13) deviated by less than 3% from the reference readings during steady-state operation.

The reactive power trace (Fig. 14) is the one notable exception to this agreement. For a purely resistive load, reactive power is theoretically close to zero, and the Fluke PQA reported near-zero values as expected. Both the DAQ system and the MECO meter, by contrast, exhibited oscillating reactive power readings that are physically inconsistent with a resistive load. In the case of the DAQ system, this behaviour is attributed to the sensitivity of the firmware's phase-angle computation to small timing jitter in the zero-crossing detection when the true phase angle is close to zero, a condition under which even minor sampling misalignment is amplified into a large apparent VAr reading. The MECO meter's larger oscillations are consistent with its known susceptibility to calibration drift under near-unity power factor conditions. While the apparent power (Fig. 15), power factor (Fig. 16), and frequency (Fig. 17) remained in close agreement with both reference instruments.

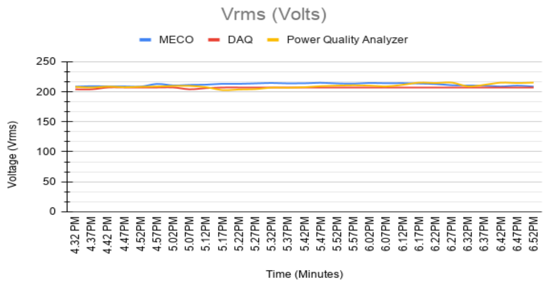

***Fig. 11**: RMS voltage*

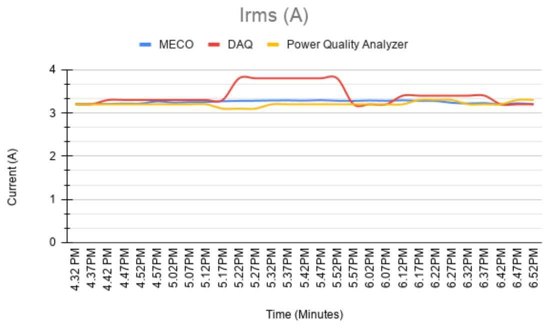

***Fig. 12:** RMS Current*

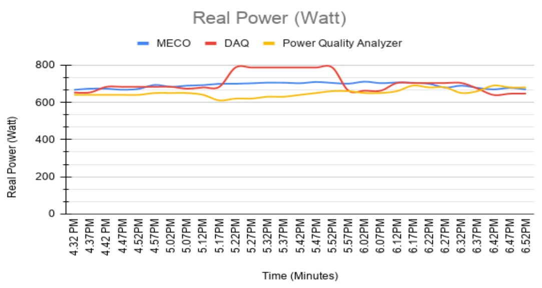

Fig. 13: *Real Power*

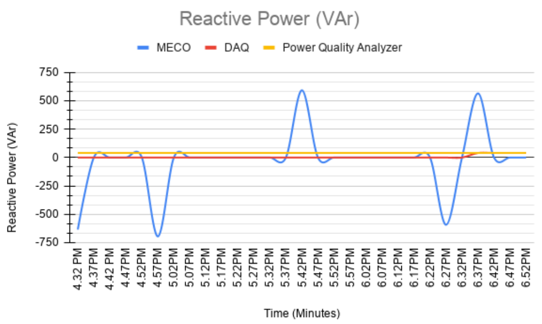

Fig. 14: *Reactive Power*

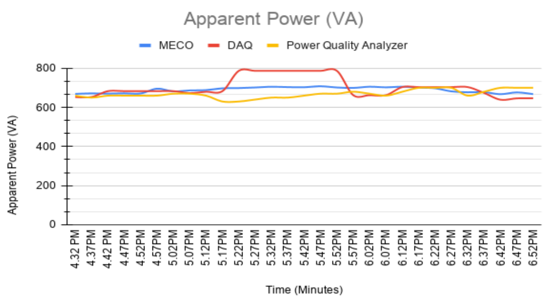

Fig. 15: *Apparent power*

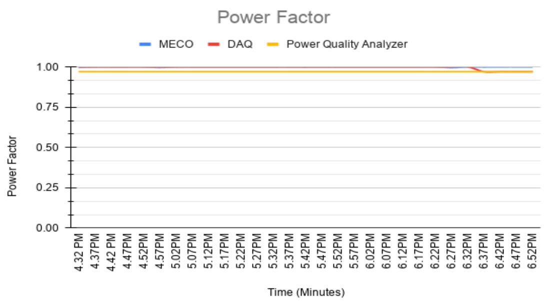

Fig. 16: *Power factor*

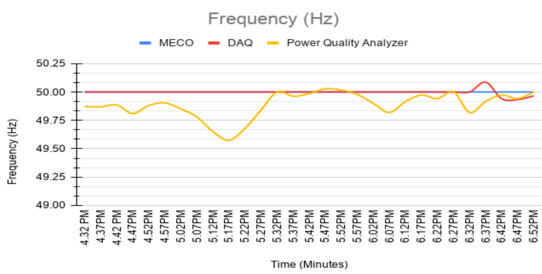

Fig. 17: *Frequency*

Table 3: *Irms*

Irms				
Comparison	MAE	MAE %	RMSE	RMSE %
DAQ vs MECO	0.181	5.548	0.265	8.148
DAQ vs PQA	0.221	6.891	0.325	9.858

Table 4: *Vrms*

Vrms				
Comparison	MAE	MAE %	RMSE	RMSE %
DAQ vs MECO	1.672	0.751	1.958	0.879
DAQ vs PQA	1.123	0.509	1.374	0.622

b. Capacitive Loads

Under capacitive loading, the DAQ current measurement remained highly accurate with a 1.37% MAE against the PQA. RMS voltage and RMS current (Fig. 18, Fig. 19) again tracked the reference instruments closely, reflecting the strong signal-to-noise ratio afforded by the higher current magnitude of the capacitor bank. Real power (Fig. 20) is small in absolute terms at this low power factor, so the percentage error is more sensitive to minor calibration offsets between instruments than under resistive or inductive loading; this explains why the relative deviation in real power is larger here than for the other two load types even though the absolute error remains modest. Reactive power (Fig. 21) and apparent power (Fig. 22) followed the expected leading-VAr profile of a capacitive load and tracked the Fluke PQA reference within the system's overall accuracy budget.

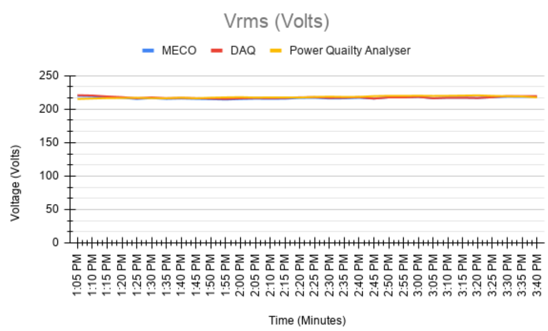

Fig. 18: *RMS voltage*

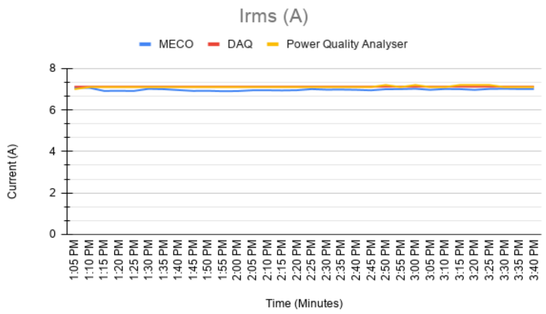

Fig. 19: *RMS current*

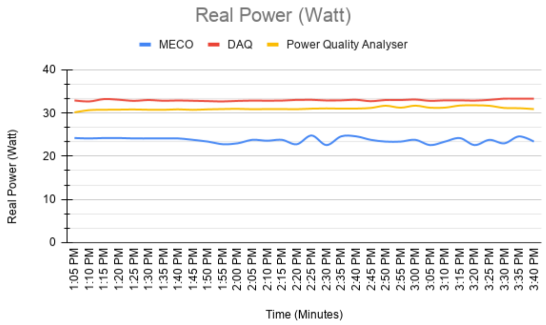

Fig. 20: *Real power*

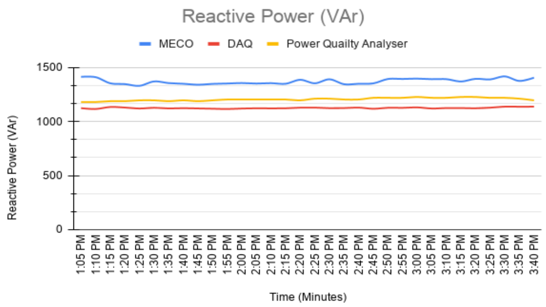

Fig. 21: *Reactive power*

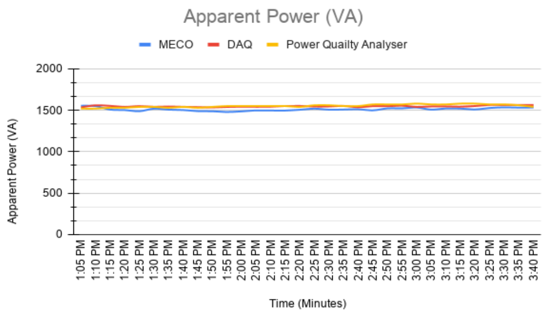

Fig. 22: *Apparent power*

c. Inductive Loads

Under inductive motor loads, the system maintained an accuracy of within 1.5% for all parameters, achieving Class 0.5 performance for voltage and apparent power. This result is best understood in relation to the two other load tests. The inductive test was run at a comparatively high and rising supply voltage (approximately 216–229 V, Fig. 23), which improved the signal-to-noise ratio of the ZMPT101B voltage-sensing channel relative to the capacitive-load test and yielded the lowest voltage error of the three load types. Because apparent power is computed directly from the product of the well-calibrated voltage and current channels (Fig. 24), its accuracy tracked the voltage channel closely, allowing both parameters to fall within the IEC Class 0.5 tolerance band specifically under this loading condition. Real and reactive power (Fig. 25, Fig. 26) remained within 1.5% of the Fluke PQA reference, power factor (Fig. 28) matched the PQA to within measurement resolution, and the DAQ system also captured a transient current inrush event and a brief grid under-frequency excursion (Fig. 27, Fig. 29) that the MECO meter's fixed-interval averaging failed to register, further supporting the system's suitability for dynamic power-quality monitoring.

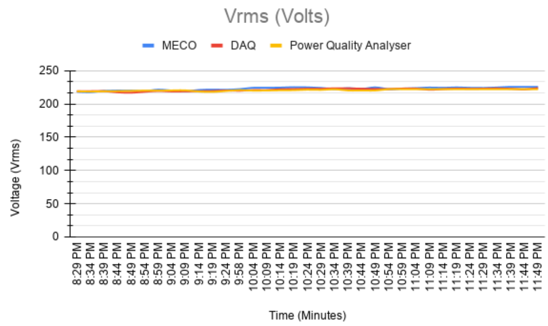

Fig. 23: *RMS Voltage*

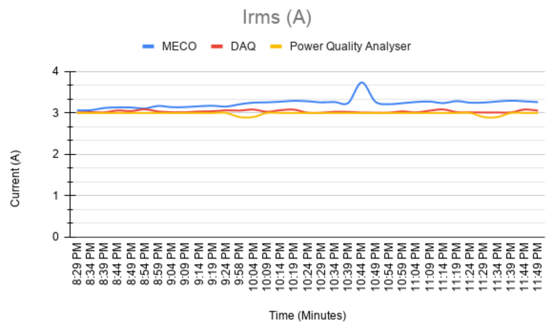

Fig. 24: *RMS Current*

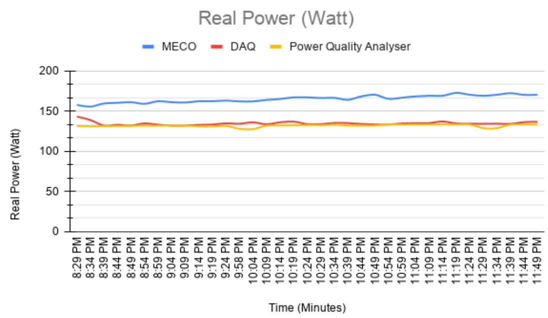

Fig. 25: *Real power*

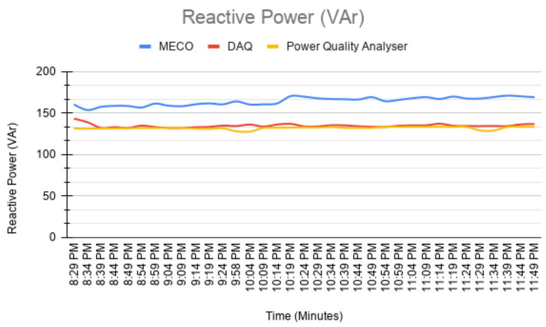

Fig. 26: *Reactive power*

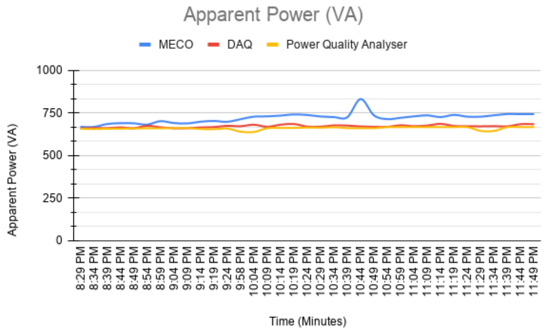

Fig. 27: *Apparent power*

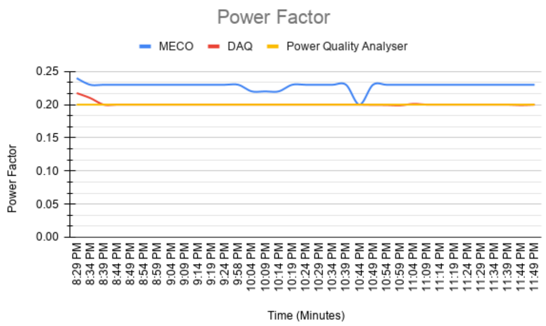

Fig. 28: *Power factor*

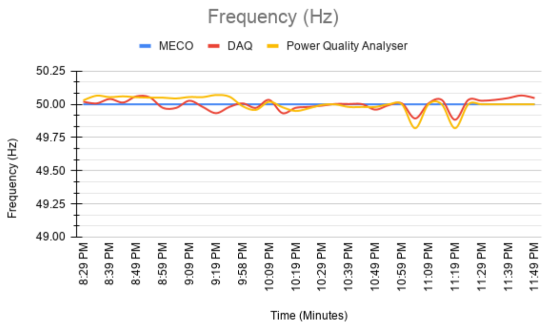

Fig. 29: *Frequency*

4.2. Power Quality and Harmonics

Harmonic analysis was performed on an induction motor via MATLAB FFT (Fig. 30, Fig. 31). The analysis identified a THD-V of 15.38% and a THD-i of 84.16%, both of which substantially exceed the IEEE Std 519-2014 individual harmonic limits. It is important to clarify that these values, together with the fundamental and harmonic magnitudes shown in Fig. 30 and Fig. 31, were extracted from a short waveform segment captured during the motor's startup transient rather than from a time-averaged steady-state window; only two complete cycles were available for the FFT, and the captured voltage and current still contained a residual startup ramp after DC-offset removal and detrending. The reported THD-V and THD-i are therefore transient-state, inrush-condition characterisations rather than steady-state compliance figures, and the abnormally large even-order harmonics (2nd and 4th) visible in both spectra reflect the waveform asymmetry introduced by the transient event and by transformer-core saturation during energisation, rather than genuine continuous-operation distortion. A well-conditioned steady-state measurement on the same load would be expected to show substantially lower THD, consistent with typical values of 1–3% (THD-V) and 3–8% (THD-i) reported for comparable inductive loads; capturing such a steady-state window is recommended as a direct extension of this work.

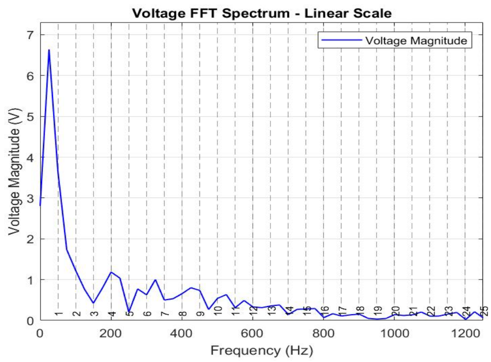

Fig. 30: *Voltage FFT Harmonic Spectrum (H1-H25)*

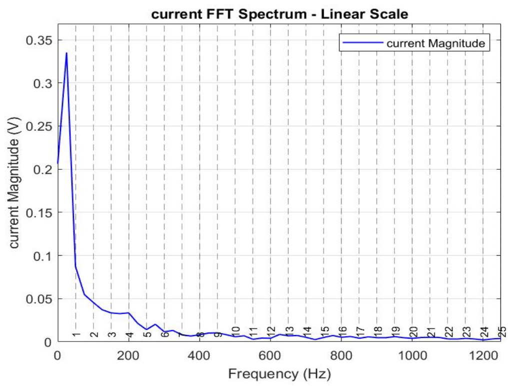

Fig. 31: *Current FFT Harmonic Spectrum (H1-H25)*

5. CONCLUSION

This study designed, implemented, and experimentally validated a low-cost, IoT-based Data Acquisition System for real-time monitoring of the JNEC distribution network, combining an Arduino Uno for local signal acquisition with an ESP32 for wireless transmission to Firebase, ThingSpeak, and Google Sheets for real-time visualisation and long-term archiving.

Across resistive, capacitive, and inductive loads, the system achieved relative errors below 1.5% for the critical electrical parameters and reached IEC Class 0.5 performance for voltage and apparent power under inductive loading, while remaining stable throughout extended testing. MATLAB-based FFT analysis further characterised the harmonic profile of an induction motor under startup-transient conditions (THD-V = 15.38%, THD-i = 84.16%), exceeding IEEE Std 519 limits as expected for inrush conditions rather than steady-state operation.

For JNEC, the system directly addresses the absence of real-time monitoring identified in the introduction, giving early visibility into voltage, current, and power-quality disturbances that helps protect sensitive laboratory equipment, reduce unplanned maintenance, and support energy auditing, while also serving as an applied learning platform for electrical engineering students.

Building on this groundwork, future work will extend the sensing architecture to three-phase monitoring, required for full campus-scale deployment on JNEC's three-phase network, and explore machine learning-based fault prediction using the harmonic and power-quality signatures identified in this study.

6. ACKNOWLEDGEMENT

The authors express sincere gratitude to Mr. Thinley Tobgay for his guidance and support throughout the project. In Addition, we would like to thank Mr. Karma Singye for timeless effort to our project. We also thank the faculty of the Department of Electrical and Electronics Engineering at JNEC.

7. REFERENCES

Ayob, M. N., Ku Ahmad Bistamam, K. M. M., Hassan Basri, H., Muhamad Azmi, M. S., Othman, S. M., & Mohamad Hashim, M. S. (2025). Development of 3-phase power measurement instrument. *International Journal of Autonomous Robotics and Intelligent Systems (IJARIS), 1*(1), 117–128. https://doi.org/10.58915/ijaris.v1i1.2366

Ferdiansyah, F., & Wardana, A. S. (2025). IoT-based real-time monitoring and energy consumption analysis for residential electrical systems. *BRIDGE: The Multidisciplinary Research Portal, 3*(1), 3025–3640.

Hamzah, A. A., & Hassan, O. A. (2024). IoT-based electrical distribution box power monitoring system using Raspberry Pi. *Progress in Engineering Application and Technology, 5*(2), 63–76. https://doi.org/10.30880/peat.2024.05.02.007

IEEE. (2014). *IEEE Std 519-2014: IEEE recommended practice and requirements for harmonic control in electric power systems.* Institute of Electrical and Electronics Engineers. https://doi.org/10.1109/IEEESTD.2014.6826459

Ildephonse, K. (2022). *Design of an IoT-based real-time data acquisition system for solar PV monitoring* [Unpublished undergraduate thesis]. University of Rwanda, ACE-IoT. https://www.aceiot.ur.ac.rw/

Pardede, J. O., & Brahmana, K. (2023). Improving reading accuracy of ACS712 current sensor with ATmega328 10-bit ADC: Enhancing resolution to 5 mA/bit via AD620 differential amplifier and Kalman filters. *Journal of Technomaterial Physics, 5*(2), 104–110. https://doi.org/10.32734/jotp.v5i2.11355

Sahabudin, N. F. A., Rusli, J. R., Ahmad, I., Kahar, N. H. A., Azmi, M. A. M., & Roslan, N. F. (2024). Development of a real-time electrical monitoring system for residential buildings. *Proceedings of the 2024 IEEE 10th International Conference on Smart Instrumentation, Measurement and Applications (ICSIMA)*, 224–228. https://doi.org/10.1109/ICSIMA62563.2024.10675545

Wibowo, A., Jayendra, I. G. B., Utari, D. Y., Rasyiid, M., & Aprilianto, R. A. (2024). Design of ACS712-based current sensing monitoring evaluation for PWM solar charge controller. *Sainteknol: Jurnal Sains Dan Teknologi, 22*(2), 80–91. https://doi.org/10.15294/sainteknol.v22i2.20604